SPECTRAL UNMIXING OF FLUORESCENCE FINGERPRINT IMAGERY FOR VISUALIZATION OF CONSTITUENTS IN PIE PASTRY

Naoto Yokoya[1]*, Mito Kokawa*[2]*, and Junichi Sugiyama*[2]

[1]Department of Advanced Interdisciplinary Studies, The University of Tokyo, Japan
[2]National Food Research Institute, National Agriculture and Food Research Organization, Japan

ABSTRACT

In this work, we present a new method that combines fluorescence fingerprint (FF) imaging and spectral unmixing to visualize microstructures in food. The method is applied to visualization of three constituents, gluten, starch, and butter, in two types of pie pastry. It is challenging to discriminate between starch and butter because both of them can be represented by similar FFs of low intensities. Two optimization approaches of FF unmixing that consider qualitative knowledge are presented and validated by comparison to the conventional staining method. Although starch and butter were represented by very similar FFs, a constrained-least-squares method with abundance quantization successfully visualized the distributions of constituents in pie pastry.

Index Terms— Fluorescence fingerprint imaging, spectral unmixing

1. INTRODUCTION

A fluorescence fingerprint (FF), which is also known as an excitation-emission matrix (EEM), is an alternative representation of the fluorescence spectra with each matrix element representing the fluorescence intensity of a given pair of excitation and emission wavelengths [1, 2]. Owing to its large amount of data, FFs can be used to discriminate between samples that have similar fluorescence properties, such as wines made in different regions [3]. Recently, FF imaging has been proved to be helpful for visualization of internal structures of foods, which is important for food monitoring [4, 5]. Conventional analytical techniques, such as principle component analysis (PCA) and spectral angle mapper (SAM), are useful for extracting information from FF images; however, there is still much room for advanced analysis to take advantage of the high dimensionality of FFs.

Hyperspectral imaging is a non-destructive imaging method that utilizes the intrinsic spectral properties of constituents, and is a common macroscopic analytical tool for food quality and safety control [6]. Spectral unmixing is a blind source separation technique actively developed in remote sensing using hyperspectral imaging [7]. Spectral unmixing refers to any process that separates the pixel spectrum into spectra of distinguishable spectral signatures, which are called *endmembers*, and abundance fractions that represent the percentage of each endmember that is present in the pixel. Many researchers have studied unmixing based on a linear spectral mixture model (LSMM), which simplifies the actual complex physical model and considers the observed spectrum as a linear combination of spectral signatures of endmembers. FF imaging is a hyperspectral imaging method in the fluorescence mode. Although several researchers worked on applying unmixing to fluorescent imaging, they are limited to the use of the fluorescence spectrum, not the FF [8, 9, 10, 11].

In this work, we present FF unmixing, which decomposes FF imaging data into endmember FFs and their abundance images, to non-destructively visualize the distributions of gluten protein, starch and butter in food. Proteins, starches and fat make the structure of food, and a visualization method of these three constituents is expected to have wide spread applications. Pie pastry is used as samples, since the three constituents are known to be distributed in relatively large clusters. Endmember FFs are extracted by a joint use of manual selection of the reference FFs and a data-driven approach that finds vertices of data simplex. We present two abundance estimation methods: one approach formulated as a constrained-least-squares problem, one using a matrix factorization technique. The effectiveness of FF unmixing is validated by comparison to the conventional staining method [12, 13].

2. MATERIALS AND METHODS

We focused on two typical types of pie pastry, puff pastry and short pastry. Although the constituents of our interests are gluten, starch, and butter, it was necessary to add the fluorescence patterns of ferulic acid and microscope slide that represents air bubbles in pastry dough, in order to obtain decent results. Therefore, we aim to decompose the FF of each pixel into the FFs and abundance fractions of five constituents, i.e., gluten, starch, butter, ferulic acid, and microscope slide.

2.1. Image Acquisition

Two types of pastry dough were cut into pieces approximately 1 cm^3, embedded in compound (3% CMC embedding

medium, iTec Science, Ibaraki, Japan) and frozen immediately in the cooling bath of a cold trap (Eyela UT-2000, Tokyo Rikakikai Co. Ltd, Tokyo, Japan) with hexane as the cooling medium. When the samples were completely frozen, the samples were sliced to 10 μm using a cryotome (CM-1900, Leica) with a Surgipath DH80HS blade (Leica). The thin slices were mounted on a microscope slide (S-8215 and S-9901, Matsunami Glass Ind., Ltd., Osaka, Japan) and kept at -20 °C until observation

FF images of two types of pastry dough and fractionated gluten were acquired with the FF imaging system, using the excitation and emission wavelengths selected with PCA. The FF images were acquired in excitation and emission wavelengths ranging from 270 to 330 nm and 350 nm to 420 nm, respectively, at 10 nm intervals.

2.2. Linear Spectral Mixture Model

The LSMM is adopted for its mathematical simplicity and physical interpretability. The LSMM assumes that an observed FF at a pixel can be expressed as a linear combination of endmember FFs:

$$y = Ea + n. \tag{1}$$

Here, $y \in \mathbb{R}^{L\times 1}$ is the observed FF reshaped into one dimension, $E \in \mathbb{R}^{L\times M}$ is the endmember FF matrix with each column vector representing an endmember FF when it is reshaped into a matrix, $a \in \mathbb{R}^{M\times 1}$ is the abundance vector, and $n \in \mathbb{R}^{L\times 1}$ is the noise vector. L is the number of combinations of excitation and emission wavelengths and M is the number of endmembers. When the LSMM is written for a whole FF image, the equation is expressed in matrix form as

$$Y = EA + N, \tag{2}$$

where $Y \in \mathbb{R}^{L\times P}$ is the whole image, $A \in \mathbb{R}^{M\times P}$ is the abundance matrix, $N \in \mathbb{R}^{L\times P}$ is the noise matrix, and P is the number of pixels. The FF unmixing problem is to decompose Y into E and A. When the number of endmembers are known, spectral unmixing is mainly composed of two steps: endmember extraction and abundance estimation.

2.3. Endmember Extraction

A condition that assumes the existence of pure pixels for all endmembers is called as *pure-pixel assumption*. In an area corresponding to a pure pixel, there is only one endmember. With this condition, the endmember spectra can be assumed to locate on the vertices of the data simplex. In this case, the estimation of endmember spectra is boiled down as the geometry-based detection of the vertices of the data simplex in high-dimensional space. Endmember extraction methods based on the pure-pixel assumption have been actively developed in remote sensing [14, 15, 16]. The vertex component analysis (VCA) algorithm is one of the most well-know geometry-based endmember extraction methods. VCA iteratively projects data samples onto a direction that is orthogonal to the subspace defined by the previously determined endmembers. The extreme point on the projection is detected as the new endmember spectrum.

Unsupervised endmember extraction methods enable finding vertices of the data simplex; however, a reference spectral library is required to determine their physical properties. We jointly use the reference FFs and VCA to extract the endmember FFs. First, we prepare the reference FFs. The reference FF of gluten is obtained from the FF image of fractionated gluten. Small areas of starch and microscope slide were manually extracted from each observed FF image. Those of butter and ferulic acid were extracted from the FF image of the puff pastry dough owing to their clear textures. All the FFs of the selected areas were averaged to acquire the reference FFs of these five endmembers. Since the variances of FFs of gluten and ferulic acid are large, their endmember FFs were chosen from similar FFs extracted by VCA. The cosine similarity is used for similarity measurement. The endmember matrix can be derived using this supervised endmember extraction.

2.4. Constrained-Least-Squares Method with Abundance Quantization

Once the endmember signatures are obtained, the abundances can be estimated by minimizing the residuals in the LSMM. Therefore, the unmixing problem is formulated as the constrained-least-squares problem [17]:

$$\begin{aligned} &\text{minimize } \tfrac{1}{2}\|y - Ea\|_2^2 \\ &\text{subject to } a \succeq 0,\ \textstyle\sum_{i=1}^{M} a_i \le 1, \end{aligned} \tag{3}$$

where the vector a is the optimization variable. The inequality notion for vectors denotes componentwise inequality. The first constraint is the nonnegativity of abundance fractions and the second constraint means that the sum of abundance fractions at the pixel is less than unit due to variability of endmember spectra. This optimization is a quadratic programming problem [18], which is written as

$$\begin{aligned} &\text{minimize } \tfrac{1}{2}a^T E^T E a - y^T E a \\ &\text{subject to } Ga \preceq h, \end{aligned} \tag{4}$$

where $G = \left[-I\ \mathbf{1}_M\right]^T$ ($\mathbf{1}_M \in \mathbb{R}^{M\times 1}$), $I \in \mathbb{R}^{M\times M}$ is the identity matrix, and $h = \left[\mathbf{0}_M^T\ 1\right]^T$ ($\mathbf{0}_M \in \mathbb{R}^{M\times 1}$).

In this work, we introduce quantization of the abundance fraction of microscope slide. When the samples were sliced, small holes were observed in the thin slice, where the microscope slide could be seen through. In this case, the abundance fraction of microscope slide can be assumed to be 0 or 1. The penalty term is added to the cost function in (3) as

$$\frac{1}{2}\|y - Ea\|_2^2 + \frac{1}{2}\lambda\left(a_{slide} - U\left(a_{slide}\right)\right)^2, \tag{5}$$

where a_{slide} is the abundance fraction of microscope slide and λ is a parameter. $U(x)$ is a step function defined as

$$U(x) = \begin{cases} 0 & \text{if } x \leq \frac{1}{2} \\ 1 & \text{otherwise.} \end{cases} \tag{6}$$

This cost function is no longer convex. Depending on the abundance fraction of microscope slide, the optimization can be divided into the two cases of quadratic programming: if $a_{slide} \leq \frac{1}{2}$,

$$\begin{aligned} &\text{minimize } \tfrac{1}{2}a^T(E^TE + \lambda C)a - y^TEa \\ &\text{subject to } G_1 a \preceq h_1, \end{aligned} \tag{7}$$

otherwise

$$\begin{aligned} &\text{minimize } \tfrac{1}{2}a^T(E^TE + \lambda C)a - (y^TE + \lambda b^T)a \\ &\text{subject to } G_2 a \preceq h_2, \end{aligned} \tag{8}$$

where $b \in \mathbb{R}^{M\times 1}$ has unit for b_{slide} and zero values for the other components and $C = bb^T$. $G_1 = \begin{bmatrix} G^T & b \end{bmatrix}^T$, $h_1 = \begin{bmatrix} h^T & 1/2 \end{bmatrix}^T$, $G_2 = \begin{bmatrix} G^T & -b \end{bmatrix}^T$ and $h_2 = \begin{bmatrix} h^T & -1/2 \end{bmatrix}^T$. In our implementation, the optimization (4) is firstly solved. Sequentially, depending on the condition of a_{slide}, the optimization (7) or (8) is solved to obtain the final result. Optimization methods for quadratic programming, such as active-set and interior-point methods, can solve (4), (7), and (8) with the global optimum. We refer to this method as the constrained-least-squares method with abundance quantization (CLSAQ).

2.5. $L_{1/2}$ Nonnegative Matrix Factorization

When we consider the nonnegativity of the matrices Y, E, and A in (2), the unmixing problem can be seen as nonnegative matrix factorization (NMF), which factorizes a nonnegative matrix into two nonnegative matrices [19]. In the last decade, NMF and its extensions have been intensively studied in hyperspectral unmixing and proved their effectiveness without the pure-pixel assumption [20, 21]. NMF was also applied to fluorescent imaging data [10]. For our problem setting, very few endmembers can be assumed to be mixed in a pixel owing to high-spatial-resolution imaging and the limited number of endmembers. Therefore, as a comparison method to CLSAQ, we adopt a sparsity constrained NMF that uses $L_{1/2}$ sparsity constraint on abundances [22]. $L_{1/2}$-NMF formulates the unmixing problem as

$$\begin{aligned} &\text{minimize } \tfrac{1}{2}\|Y - EA\|_F^2 + \eta\|A\|_{1/2} \\ &\text{subject to } E \succeq 0,\ A \succeq 0,\ \textstyle\sum_{i=1}^{M} a_i \leq 1, \end{aligned} \tag{9}$$

with variables E and A, where $\|\cdot\|_F$ denotes the Frobenius norm, $\|A\|_{1/2}$ is the summation of square roots of all elements in A and η is the parameter. This optimization is guaranteed to converge to local optima using the multiplicative update rules as follows:

$$\begin{aligned} E &\leftarrow E. * YA^T./EAA^T \\ A &\leftarrow A. * E^TY./\left(E^TEA + \tfrac{\eta}{2}A^{-\frac{1}{2}}\right), \end{aligned} \tag{10}$$

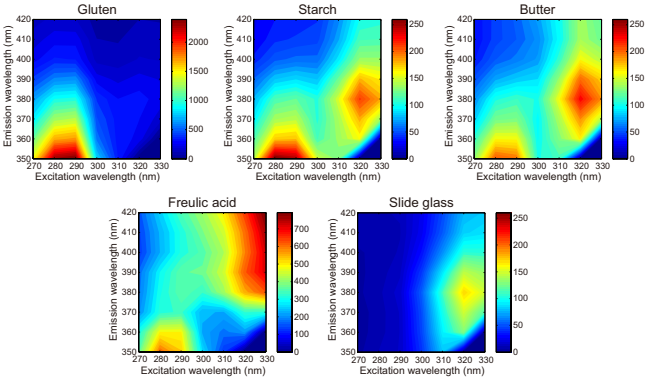

Fig. 1. Endmember FFs of short pastry dough.

where .* and ./ denote elementwise multiplication and division, respectively. E and A are initialized using the extracted endmember FFs and a matrix with constant values, respectively. To satisfy the additivity constraint, we add the black spectrum to E, and the data matrix Y and the endmember FF matrix E are augmented by a row of constants defined by $\tilde{Y} = \begin{bmatrix} Y^T & \delta \mathbf{1}_P \end{bmatrix}^T$ and $\tilde{E} = \begin{bmatrix} E^T & \delta \mathbf{1}_P \end{bmatrix}^T$, respectively, where δ controls the impact of the additivity constraint [17].

3. EXPERIMENTAL RESULTS

Fig. 1 shows the endmember FFs used for the short pastry dough. Gluten and ferulic acid have characteristic fluorescence patterns, whereas those of starch and butter are very similar. Although starch itself is not fluorescent, starch granules are known to be surrounded by a protein membrane. The FF of starch is a mixture of the protein FF and the FF of the microscopy slide which passes through the starch granule. The microscope slides are not completely fluorescence free and show weak fluorescence.

Fig. 2 shows the abundance images of gluten, starch, butter, ferulic acid, and microscope slide obtained by CLSAQ and $L_{1/2}$-NMF. The top two rows are the results of the short pastry dough and the bottom two rows are those of the puff pastry dough, which shows a band of butter sandwiched between two layers of wheat dough. As shown in the first and third rows obtained by CLSAQ, abundances for microscope slide are shown in black (abundance=0) and white (abundance=1), whereas the other constituents are shown in continuum values between 0 and 1. Even though the FFs of starch and butter are similar, there are obvious differences between their distributions for both pastry dough. Particularly, in the abundance image of starch for the puff pastry dough, starch particles are visualized. As shown in the second and fourth rows obtained by $L_{1/2}$-NMF, the abundance images of gluten and ferulic acid are very similar to those of CLSAQ; however, it is difficult to distinguish those of starch and butter for the short pastry dough and starch particles are failed to be visualized for the puff pastry dough. These results indicate

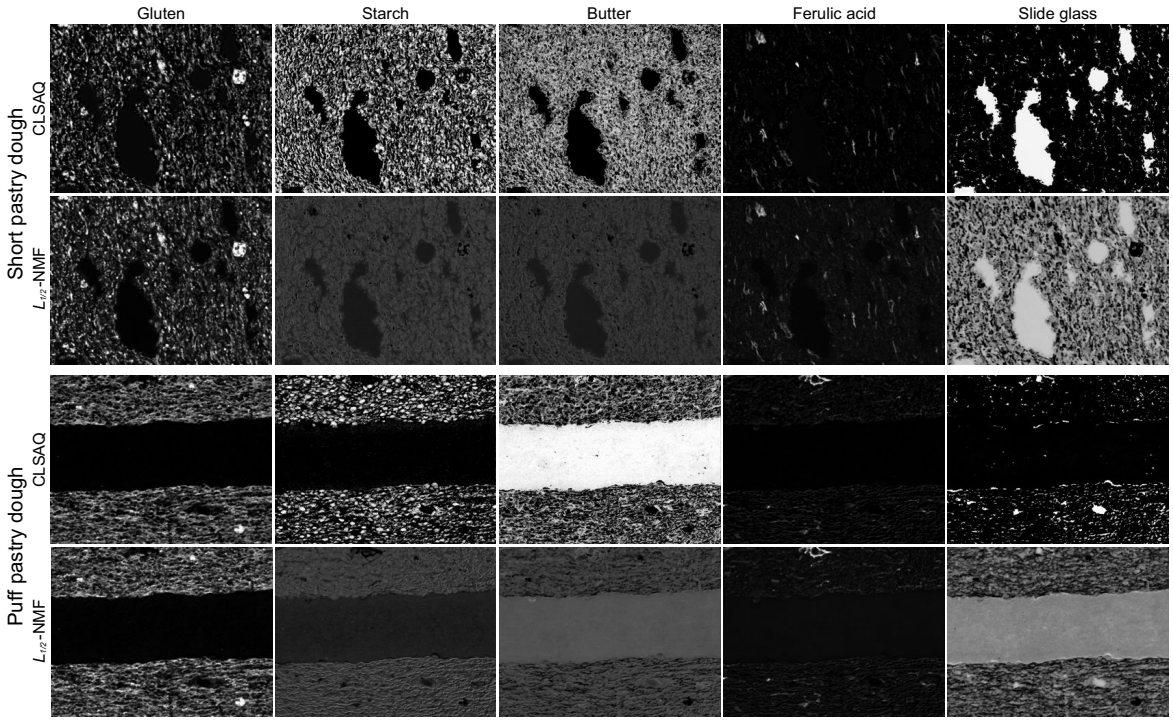

Fig. 2. Abundance images of gluten, starch, butter, ferulic acid, and microscope slide from left to right columns for short pastry dough on top two rows and puff pastry dough on bottom two rows.

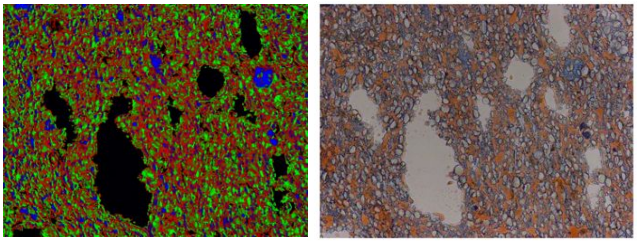

Fig. 3. (Left) Composite image of the abundance images of butter (red), starch (green) and gluten (blue) obtained by CLSAQ. (Right) Stained image of the same sample. Protein is stained blue and fat is stained orange.

that it is important to place high priority on the reference FFs carefully selected using human knowledge when endmember FFs are very similar.

In order to validate the analysis results, the short pastry was stained. Fig. 3 shows the composite image obtained by CLSAQ assigning the abundance images of butter, gluten, and starch to red, blue, and green, respectively, and the stained image. Large aggregates of gluten can be observed in both images and the positions of starch granules and fat in the analyzed image are largely correspondent with those of the stained image. The FFs of starch and butter were difficult to distinguish by visual judgmental; however, it was possible to obtain their abundances accurately. Fluorescence intensity would be proportional to the volume of these constituents. In the short pastry, the volume ratio calculated from the weights and specific gravities of the ingredients is 12.9%:37.8%:49.3% for gluten, starch, and butter ratio. On the other hand, the ratios calculated from the abundance matrices obtained by CLSAQ and $L_{1/2}$-NMF were 16.6%:37.6%:45.8% and 30.8%:36.3%:32.9%, respectively. The ratio obtained by CLSAQ is very close to that calculated from the ingredients of pie pasty, and seems to support the accuracy of CLSAQ.

4. CONCLUSION

We have presented spectral unmixing of FF images to visualize distributions of the constituents in pie pastry. The experimental results showed that the constrained-least-squares method with abundance quantization successfully visualize the abundance distributions of five endmembers even though there are very similar FFs. FF unmixing enables non-destructive visualization of microstructures in biological imaging, and can be expected to be an alternative tool of staining.

5. ACKNOWLEDGEMENT

The authors thanks Ms. Hiroko Ashida (Fuji Oil Co., Japan) for providing the experimental data.

6. REFERENCES

[1] D. W. Johnson, J. B. Callis, and G. D. Christian, "Rapid scanning fluorescence spectroscopy," *Anal. Chem.*, vol. 49, no. 8, pp. 747A–757A, 1977.

[2] B. J. H. Matthews, A. C. Jones, N. K. Theodorou, and A. W. Tudhope, "Excitation-emission-matrix fluorescence spectroscopy applied to humic acid bands in coral reefs," *Marine Chemistry*, vol. 55, pp. 317–332, 1996.

[3] C. Yin, H. Li, C. Ding, and H. Wang, "Preliminary investigation on variety, brewery and vintage of wines using three-dimensional fluorescence spectroscopy," *Food Science and Technology Research*, vol. 15, no. 1, pp. 27–38, 2009.

[4] M. Tsuta, K. Miyashita, T. Suzuki, S. Nakauchi, Y. Sagara, and J. Sugiyama, "Three-dimensional visualization of internal structural changes in soybean seeds during germination by excitation-emission matrix imaging," *Transactions of American Society of Agricultural and Biological Engineers*, vol. 50, no. 6, pp. 2127–2136, 2007.

[5] M. Kokawa, K. Fujita, J. Sugiyama, M. Tsuta, M. Shibata, T. Araki, and H. Nabetani, "Quantification of the distributions of gluten, starch and air bubbles in dough at different mixing stages by fluorescence fingerprint imaging," *Journal of Cereal Science*, vol. 55, pp. 15–21, 2012.

[6] A. A. Gowen, C. P. O'Donnell, P. J. Cullen, G. Downey, and J. M. Frias, "Hyperspectral imaging–an emerging process analytical tool for food quality and safety control," *Trends in Food Sciend and Technology*, vol. 18, pp. 590–598, 2007.

[7] J. M. Bioucas-Dias, A. Plaza, N. Dobigeon, M. Parente, Q. Du, P. Gader, and J. Chanussot, "Hyperspectral unmixing overview: geometrical, statistical, and sparse regression-based approaches," *IEEE J. Sel. Topics Appl. Earth Observ. Remote Sens.*, vol. 5, no. 2, pp. 354–379, 2012.

[8] T. Zimmermann, "Spectral imaging and linear unmixing in light microscopy," *Adv. Biochem. Engin./Biotechnol.* vol. 95, pp. 245–265, 2005.

[9] B. Kraus, M. Ziegler, and H. Wolff, "Linear fluorescence unmixing in cell biological research," *Modern Research and Educational Topics in Microscopy (ed. by A. Mendez-Vilas and J. Diaz)*, pp. 863–872, 2007.

[10] R. A. Neher, M. Mitkovski, F. Kirchhoff, E. Neher, F. J. Theis, and A. Zeug, "Blind source separation techniques for the decomposition of multiply labeled fluorescence images," *Biophysical Journal*, vol. 96, pp. 3791–3800, 2009.

[11] F. Fereidouni, A. N. Bader, and H. C. Gerritsen, "Spectral phasor analysis allows rapid and reliable unmixing of fluorescence microscopy spectral images," *Optics Express*, vol. 20, no. 12, pp. 12729–12741, 2012.

[12] F. Auger, M. H. Morel, J. Lefebvre, M. Dewilde, and A. Redl, "A parametric and microstructural study of the formation of gluten network in mixed flour-water batter," *Journal of Cereal Science*, vol. 48, no. 2, pp. 349–358, 2008.

[13] T. Maeda, M. Kokawa, M. Miura, T. Araki, M. Yamada, K. Takeya, and Y. Sagara, "Development of a novel staining procedure for visualizing the gluten–starch matrix in bread dough and cereal products," *Cereal Chem.*, vol. 90, no. 3, pp. 175–180, 2013.

[14] J. W. Boardman, "Automating spectral unmixing of AVIRIS data using convex geometry concepts," *Proc. Ann. JPL Airborne Geosci. Workshop*, vol. 1, pp. 11–14, 1993.

[15] M. E. Winter, "N-findr: An algorithm for fast autonomous spectral end-member determination in hyperspectral data," *Proc. SPIE*, vol. 3753, pp. 266–275, 1999.

[16] J. M. P. Nascimento and J. M. B. Dias, "Vertex component analysis: A fast algorithm to unmix hyperspectral data," *IEEE Trans. Geosci. Remote Sens.*, vol. 43, no. 4, pp. 898–910, 2005.

[17] D. C. Heinz and C.-I. Chang, "Fully constrained least squares linear spectral mixture analysis method for material quantification in hyperspectral imagery," *IEEE Trans. Geosci. Remote Sens.*, vol. 39, no. 3, pp. 529–545, Mar. 2001.

[18] S. Boyd and L. Vandenberghe, *Convex Optimization*. Cambridge, U.K.: Cambridge Univ. Press, 2004.

[19] D. D. Lee and H. S. Seung, "Learning the parts of objects by nonnegative matrix factorization," *Nature*, vol. 401, pp. 788–791, 1999.

[20] L. Miao and H. Qi, "Endmember extraction from highly mixed data using minimum volume constrained nonnegative matrix factorization," *IEEE Trans. Geosci. Remote Sens.*, vol. 45, no. 3, pp. 765-777, 2007.

[21] S. Jia and Y. Qian, "Constrained nonnegative matrix factorization for hyperspectral unmixing," *IEEE Trans. Geosci. Remote Sens.*, vol. 47, no. 1, pp. 161-173, 2009.

[22] Y. Qian, S. Jia, J. Zhou, and A. Robles-Kelly, "Hyperspectral unmixing via $L_{1/2}$ sparsity-constrained nonnegative matrix factorization, " *IEEE Trans. Geosci. Remote Sens.*, vol. 49, no. 11, pp. 4282–4297, 2011.